Nanoscale

PAPER

View Article Online
View Journal

Cite this: DOI: 10.1039/d5nr04734j

Visible-light-driven antibacterial activity of poly (3-hexylthiophene-2,5-diyl) nanoparticles

Tomoka Ishikawa,†[a] Aki Shibata,†[a] Hitoshi Kasai [a] and Kouki Oka *[a,b,c]

Sterilisation using photocatalysts does not lead to the development of drug-resistant bacteria and has therefore attracted significant attention. Particularly, organic semiconductors typically comprise earth-abundant elements and allow facile tuning of their material properties through organic synthesis. A representative organic semiconductor, poly(3-hexylthiophene-2,5-diyl) (**P3HT**), exhibits visible-light absorption and efficient charge-transport properties owing to its π-conjugated structure, emphasising its potential for visible-light-driven photocatalysis. However, the hydrophobic nature of **P3HT** makes it difficult to employ in aqueous environments conducive to bacterial growth while maintaining its chemical structure. In this work, to investigate the antibacterial activity of hydrophobic organic semiconductors in aqueous environments, **P3HT** nanoparticles (**NPs**) with diameters ranging approximately 40–100 nm were prepared *via* reprecipitation, enabling stable dispersion in aqueous solution while maintaining the molecular structure of **P3HT**. **P3HT NPs** with higher regioregularity and larger specific surface areas generate greater amounts of reactive oxygen species and exhibit an enhanced antibacterial activity. **P3HT NPs** with 99% regioregularity and an average particle diameter of 42 nm achieved a sterilisation rate of 99% against *E. coli* after 6 h of visible-light irradiation. This work demonstrates that predominantly hydrophobic organic semiconductors can be developed as photocatalysts capable of sterilisation in aqueous environments through **NP** formation.

Received 9th November 2025,
Accepted 18th March 2026

DOI: 10.1039/d5nr04734j

rsc.li/nanoscale

Introduction

Bacteria are microorganisms capable of self-replication, and among them, pathogenic species can invade and multiply within the human body, leading to infections.[1] Since antibiotics targeting infections caused by various pathogenic bacteria have been developed, humans have been able to protect themselves from numerous infectious diseases.[2] However, the excessive use of antibiotics has led to the emergence of antimicrobial-resistant (**AMR**) bacteria.[3,4] The global number of deaths caused by **AMR** infections is estimated to reach 10 million annually by 2050.[5] To prevent the emergence of **AMR** bacteria, minimising the use of antibiotics is essential. As an alternative sterilisation approach to antibiotics, photocatalytic methods powered by readily available sunlight (particularly visible light) have attracted considerable attention.[6,7] The sterilisation mechanism by photocatalysts is illustrated in Fig. 1(A). First, electrons in the photocatalyst are excited by light irradiation, generating reactive oxygen species (**ROS**) such as superoxide ($O_2^{\bullet-}$). Next, the generated **ROS** and photocatalyst hole oxidatively decompose bacterial cells.[8]

Since semiconductors excite electrons when the energy of the irradiating light exceeds the intrinsic bandgap of materials, they are widely used as photocatalytic materials. Among these materials, organic semiconductors offer the facile tuning of their material properties through organic synthesis[9–11] and the incorporation of earth-abundant elements.[9,12–19] **P3HT** (Fig. 1(B)) possesses a narrow bandgap of approximately 1.9–2.3 eV,[9,20] enabling the generation of **ROS** under visible light.[21] Conversely, the strong visible-light absorption capability resulting from this narrow bandgap, as compared to other π-conjugated polymers[8,22–28] shown in Fig. 1(C), is expected to yield antibacterial activity under low-energy light with longer absorption edges. In addition, high regioregular **P3HT** typically exhibits high charge mobility[29] due to strong π–π stacking interactions, which are anticipated to enhance **ROS** generation more effectively. These characteristics make **P3HT** suitable for use as a visible-light-driven photocatalyst; however, its poor water solubility limits its application in aqueous environments while retaining its chemical structure.

In this work, **P3HT NPs** are prepared using the reprecipitation method, enabling their stable dispersion in water while

[a]*Institute of Multidisciplinary Research for Advanced Materials, Tohoku University, 2-1-1 Katahira, Aoba-ku, Sendai, Miyagi 980-8577, Japan. E-mail: oka@tohoku.ac.jp*
[b]*Carbon Recycling Energy Research Center, Ibaraki University, 4-12-1, Nakanarusawacho, Hitachi, Ibaraki 316-0033, Japan*
[c]*Deuterium Science Research Unit, Center for the Promotion of Interdisciplinary Education and Research, Kyoto University, Yoshida, Sakyo-ku, Kyoto 606-8501, Japan*
†These authors contributed equally.

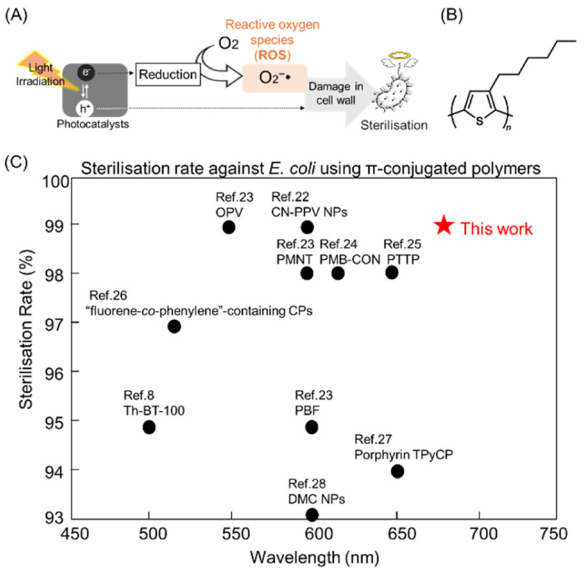

Fig. 1 (A) Schematic of photocatalytic sterilisation mechanism. (B) Molecular structure of **P3HT**. (C) Relationship between the sterilisation rate and absorption edge of π-conjugated polymers reported in the literature,[8,22–28] used as photocatalysts. The plotted values correspond to the highest sterilisation rate reported under the respective irradiation conditions.

maintaining the molecular structure of **P3HT**, thereby allowing functional development in aqueous environments. The antibacterial activity of **P3HT NPs** is investigated under visible-light irradiation. In addition, the effects of **P3HT** regioregularity and the specific surface area of the **NPs** on their antibacterial activity are analysed.

Results and discussion

Preparation and characterisation of P3HT NPs

For this study, regioregular **P3HT** (**rrP3HT**, 99% regioregularity) and regiorandom **P3HT** (**rraP3HT**, 50% regioregularity) were selected, as they exhibit distinct visible-light absorption properties (Fig. 2(A) and (E)). To adapt **P3HT** to aqueous environments for efficient sterilisation, employing a method that maximises the specific surface area of **P3HT** available for **ROS** generation at the water interface was essential. Among available techniques, the reprecipitation method[30] was selected as the optimal method because the particle size could be controlled in the range of tens nm to hundreds nm by changing the compound concentrations, and the specific surface area in water could be adjusted.[31–34] Therefore, as shown in Fig. 2(B), an aqueous dispersion of **P3HT NPs** (10–60 μM) was prepared by injecting a tetrahydrofuran (THF, good solvent) solution of **P3HT** into ultrapure water (poor solvent).

The morphology and particle size of the prepared **rrP3HT** and **rraP3HT NPs** were characterised using scanning electron microscopy (SEM) and dynamic light scattering (DLS). As shown in Fig. 2(C), the **P3HT NPs** exhibited a spherical mor-

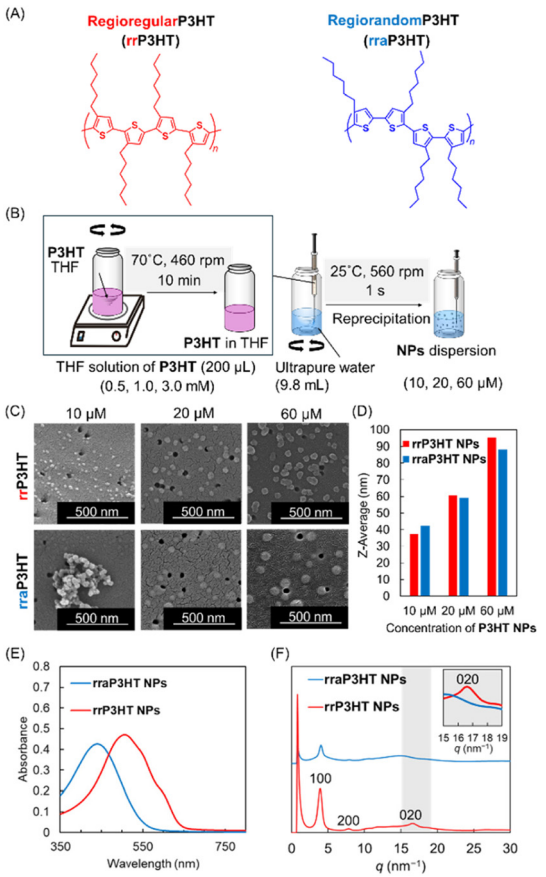

Fig. 2 (A) Molecular structure of **rrP3HT** and **rraP3HT**. (B) Preparation procedure of **P3HT NPs** dispersion using the reprecipitation method. (C) SEM images of **P3HT NPs** at 10–60 μM. (The black spots in the image are the pores of the membrane filter.) The aggregation of **NPs** observed in the SEM images was attributed to the removal of water through the filter pores, as the **NPs** were brought together on the membrane surface during this process. (D) *Z*-Average particle size of **P3HT NPs** dispersion in water measured by DLS. (E) UV–visible absorption spectrum of **P3HT NPs** dispersion. (F) WAXS intensity of **P3HT NPs** as a function of the module of the scattering vector $q = 4\pi(\sin\theta)/\lambda$.

phology, and they became smaller as the polymer concentration decreased. Similarly, as shown in Fig. 2(D), the average particle size of **NPs** in water, as measured by DLS, decreased with solution concentration, enabling the preparation of **NPs** with diameters ranging approximately 40–100 nm. **NPs** smaller than 40 nm aggregated immediately after preparation due to an increase in surface energy; therefore, **NPs** of 40 nm or larger were used to ensure stable dispersibility. The prepared **NPs** were monodispersed (Fig. S2(A) and (B)). Despite the hydrophobic nature of the **NPs** (Fig. S9 and Table S4), the **NPs** maintained a stable dispersion for at least one week (Table S2). This is presumably due to the steric repulsion caused by hydrophobic chains of **P3HT**[35] present on the surface of **NPs** composed solely of **P3HT** prepared by the reprecipitation method. In addition to steric repulsion, the stable dispersion state was maintained by the zeta potential of approximately −20 mV (Fig. S2(C) and (D)) generated by the

adsorption of hydroxide ion on the surface of **NPs** in ultrapure water.[36–38]

Since the antibacterial activity of **P3HT NPs** was evaluated under visible-light irradiation using the **NPs** dispersion, the UV–visible absorption behaviour of the dispersion was measured. As shown in the absorption spectra in Fig. 2(E), the **rrP3HT NPs** exhibited a shoulder peak near 600 nm attributed to π–π stacking interactions,[39] and a major absorption peak near 525 nm. The **rraP3HT NPs** exhibited a maximum absorption wavelength near 450 nm. Both types of **P3HT NPs** exhibited visible-light absorption and generated **ROS** under visible-light irradiation, with **rrP3HT NPs** showing stronger visible-light absorption. Additionally, to investigate the crystallinity of the **P3HT NPs**, the samples were analysed using wide-angle X-ray scattering (WAXS). As shown in Fig. 2(F), the primary diffraction peaks corresponding to the (100) and (200) planes of the **rrP3HT** and **rraP3HT NPs** were nearly identical. However, at q = 15–19 nm^{-1}, only the **rrP3HT NPs** exhibited a (020) peak[40] at 16.5 nm^{-1} attributed to π–π stacking interactions, indicating that the high regioregular **rrP3HT NPs** partially possessed a crystalline structure.

Notably, the coexistence of crystalline and amorphous structures in facilitated **P3HT** electron–hole separation[41] and suppressed charge recombination.[42] Therefore, **rrP3HT NPs** were expected to possess longer excited-electron lifetimes than the **rraP3HT NPs**.

Evaluation of the antibacterial activity of P3HT NPs

The antibacterial activities of the **rrP3HT** and **rraP3HT NPs** with high dispersion stability were evaluated under visible-light irradiation (30 mW cm^{-2}, 385–740 nm). This light intensity was selected to evaluate the differences in antibacterial activity while ensuring reproducible results and suppressing heat generation. As shown in Fig. 3(A), after visible-light irradiation of a sample containing a mixture of *E. coli* and **NPs** dispersions in LB medium for 6 h, the sterilisation rate was determined by counting the bacterial colonies that formed in agar plates. As shown in Fig. 3(B), the **rrP3HT NPs** (diameter 79 nm) achieved a 47% sterilisation rate, which was 1.6 times higher than that of the **rraP3HT NPs** (diameter 78 nm, sterilisation rate 30%) with nearly identical particle size and specific surface area. To verify whether the antibacterial activity of **P3HT NPs** originates from **ROS**, the total amount of **ROS** was quantified using the OxiSelect In Vitro ROS/RNS Assay Kit, as shown in Fig. S4(B). In the measurements, the total amount of **ROS** was quantified by measuring the fluorescence intensity of 2′,7′-dichlorofluorescein (**DCF**) generated from 2′,7′-dichlorodihydrofluorescein (**DCFH**) oxidized by **ROS**.[44] While this method does not allow for the identification of specific **ROS** species, it revealed that the **rrP3HT NPs** generated a greater amount of **ROS** compared to the **rraP3HT NPs**. Overall, the obtained results indicated that the **rrP3HT NPs**, possessing high regioregularity and pronounced π–π stacking interactions, exhibited strong visible-light absorption and suppressed electron–hole recombination,[35] thereby generating more **ROS** than the **rraP3HT NPs**.

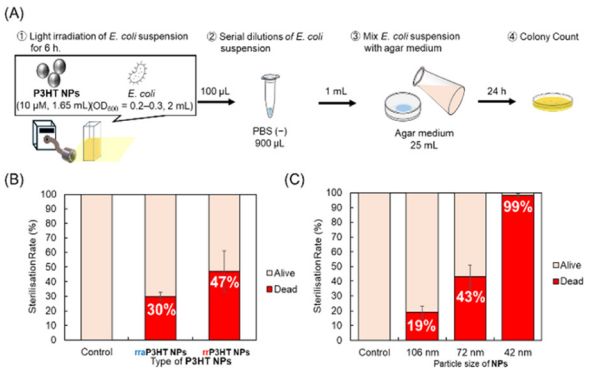

Fig. 3 (A) Experimental protocol for the pour plate method: suspensions of *E. coli* and the samples were irradiated with visible light for 6 h. Subsequently, the irradiated samples were serially diluted 10^6-fold in PBS to prevent **ROS**-induced bacterial aggregation.[43] These diluted samples were then mixed with agar medium to form colonies for counting. Control samples, which contained THF (2% v/v) at a concentration equivalent to the residual level in the **NPs** dispersions, were subjected to the same light irradiation conditions. Consequently, any potential photothermal effect induced by irradiation was accounted for as a common background factor across all samples. Antibacterial activity is evaluated by the sterilisation rate calculated from the resulting colonies. (B) The sterilisation rate of **rrP3HT NPs** and **rraP3HT NPs** (diameter about 80 nm) dispersion after visible-light irradiation (385–740 nm, 30 mW cm^{-2}, 6 h). The effects of molecular weight and residual THF, along with results under dark conditions, are shown in Fig. S5, S6 and Table S3. These were found not to be the dominant factors, and **P3HT NPs** themselves exhibited no antibacterial activity under dark conditions. (C) The sterilisation rate of **rrP3HT NPs** (42, 72, 106 nm) dispersion after visible-light irradiation (385–740 nm, 30 mW cm^{-2}, 6 h).

The antibacterial activity of the **rrP3HT NPs** was expected to be further enhanced by an increase in specific surface area. Therefore, the sterilisation rates of the **rrP3HT NPs** (average particle size: 42, 72, 106 nm) with different specific surface areas were compared. As shown in Fig. 3(C), the sterilisation rate of the **rrP3HT NPs** increased as the **NPs** became smaller. The **P3HT NPs** with high regioregularity (99%) and a large specific surface area (42 nm in diameter) exhibited a high sterilisation rate of 99%. When the sterilisation rate was plotted against specific surface area and particle number (Fig. S7), a linear relationship was observed in the range of approximately 40–100 nm (Fig. S8). (**NPs** smaller than 40 nm could not be evaluated for antibacterial activity as they aggregated immediately in the aqueous medium. Moreover, for this plot, the specific surface area was calculated by assuming the **NPs** as ideal spheres because the particle sizes used for our evaluation were obtained from DLS measurements, which themselves are based on a first-order approximation of ideal spheres.[36]) This correlation suggests that the increased specific surface area and particle number facilitated the efficient generation of the total amount of **ROS** and enhanced its interaction with *E. coli*.[22,45,46] In this work, *E. coli* (Gram-negative bacteria) was used for the initial proof-of-concept regarding the antibacterial activity of **NPs** composed of organic photocatalysts. In addition, it has been reported that in the **ROS**-driven bacteri-

cidal mechanism, the antibacterial activity against Gram-positive bacteria is equivalent to or higher than that against Gram-negative bacteria.[47–49] Based on the above, the **P3HT NPs** are expected to exhibit potential sterilisation rates against Gram-positive bacteria that are comparable to or higher than the results obtained with *E. coli*. This achievement is significant as it demonstrates high antibacterial activity utilizing longer wavelengths (a longer absorption edge) compared to those of other π-conjugated polymers. As shown in Fig. 1(C), this performance is comparable to or higher than the values reported for other π-conjugated polymers.

Conclusion

In this work, leveraging the principle that reducing the concentration of the **P3HT** solution injected into water results in smaller **NP** sizes, **P3HT NPs** were prepared with diameters ranging from approximately 40 to 100 nm. The **rrP3HT NPs** exhibited visible-light absorption and partial crystallinity arising from strong π–π stacking interactions. The **rrP3HT NPs** exhibited a higher sterilisation rate than the **rraP3HT NPs** because their strong visible-light absorption and suppression of electron–hole recombination, resulting from pronounced π–π stacking interactions, enhanced **ROS** generation under visible-light irradiation. Additionally, the smaller particle size of the **rrP3HT NPs** led to a higher sterilisation rate. The **P3HT NPs** with high regioregularity (99%) and a large specific surface area (42 nm in diameter) exhibited a high sterilisation rate of 99%. Therefore, this work demonstrated that typically hydrophobic organic semiconductors can be developed as organic photocatalysts capable of promoting sterilisation in aqueous environments through **NP** formation.

Author contributions

Tomoka Ishikawa: formal analysis, data curation, investigation, and writing – original draft & editing. Aki Shibata: writing – original draft, review and editing, supervision, resources and funding acquisition. Hitoshi Kasai: writing – review & editing, resources and funding acquisition. Kouki Oka: conceptualization, methodology, supervision, resources, writing – original draft, review and editing, funding acquisition and project administration. All of the authors discussed the results and helped in writing the manuscript.

Conflicts of interest

The authors declare no competing financial interests.

Data availability

The data supporting the findings of this work are available within the article and its supplementary information (SI). Supplementary information is available. See DOI: https://doi.org/10.1039/d5nr04734j.

Acknowledgements

This work was supported by JSPS Grants-in-Aid for Scientific Research (No. JP23K17945, JP23H03827, JPJSBP120258801, 24K01552, 25K21722, 22H00328 and JP25K23579) from MEXT, Japan. Kouki Oka also acknowledges the support from Shorai Foundation for Science and Technology, the TEPCO Memorial Foundation, the Amano Industry Technology Laboratory, Sugiyama Houkoukai, the Yamada Science Foundation, the Kenjiro Takayanagi Foundation, the Kansai Research Foundation for Technology Promotion, the Yashima Environment Technology Foundation, the JACI Prize for Encouraging Young Researchers, the Iketani Science and Technology Foundation, the Foundation for Interaction in Science & Technology, and the Kato Foundation for Promotion of Science (KS-3416), Ozawa and Yoshikawa Memorial Electronics Research Foundation, the Noguchi Institute (NJ202411). Aki Shibata also acknowledges the support from Yamaguchi Educational and Scholarship Foundation, Mishima Kaiun Memorial Foundation.

The synchrotron radiation experiments in this study were conducted at the NanoTerasu BL08W-WAXS beamline of the Photon Science Innovation Center (PhoSIC) under the Coalition Program. The experiments were made possible with the valuable assistance of PhoSIC technical staff members Mr. Haruki Meguro.

References

1 M. Rai, A. Yadav and A. Gade, *Biotechnol. Adv.*, 2009, **27**, 76–83.
2 B. P. Alcock, A. R. Raphenya, T. T. Y. Lau, K. K. Tsang, M. Bouchard, A. Edalatmand, W. Huynh, A. V. Nguyen, A. A. Cheng, S. Liu, S. Y. Min, A. Miroshnichenko, H. K. Tran, R. E. Werfalli, J. A. Nasir, M. Oloni, D. J. Speicher, A. Florescu, B. Singh, M. Faltyn, A. Hernandez-Koutoucheva, A. N. Sharma, E. Bordeleau, A. C. Pawlowski, H. L. Zubyk, D. Dooley, E. Griffiths, F. Maguire, G. L. Winsor, R. G. Beiko, F. S. L. Brinkman, W. W. L. Hsiao, G. V. Domselaar and A. G. McArthur, *Nucleic Acids Res.*, 2020, **48**, D517–D525.
3 A. P. Magiorakos, A. Srinivasan, R. B. Carey, Y. Carmeli, M. E. Falagas, C. G. Giske, S. Harbarth, J. F. Hindler, G. Kahlmeter, B. Olsson-Liljequist, D. L. Paterson, L. B. Rice, J. Stelling, M. J. Struelens, A. Vatopoulos, J. T. Weber and D. L. Monnet, *Clin. Microbiol. Infect.*, 2012, **18**, 268–281.
4 S. K. Ahmed, S. Hussein, K. Qurbani, R. H. Ibrahim, A. Fareeq, K. A. Mahmood and M. G. Mohamed, *J. Med. Surg. Public Health*, 2024, **2**, 10081.

5 C. J. L. Murray, K. S. Ikuta, F. Sharara, L. Swetschinski, G. Robles Aguilar, A. Gray, C. Han, C. Bisignano, P. Rao, E. Wool, S. C. Johnson, A. J. Browne, M. G. Chipeta, F. Fell, S. Hackett, G. Haines-Woodhouse, B. H. Kashef Hamadani, E. A. P. Kumaran, B. McManigal, S. Achalapong, R. Agarwal, S. Akech, S. Albertson, J. Amuasi, J. Andrews, A. Aravkin, E. Ashley, F.-X. Babin, F. Bailey, S. Baker, B. Basnyat, A. Bekker, R. Bender, J. A. Berkley, A. Bethou, J. Bielicki, S. Boonkasidecha, J. Bukosia, C. Carvalheiro, C. Castañeda-Orjuela, V. Chansamouth, S. Chaurasia, S. Chiurchiù, F. Chowdhury, R. Clotaire Donatien, A. J. Cook, B. Cooper, T. R. Cressey, E. Criollo-Mora, M. Cunningham, S. Darboe, N. P. J. Day, M. De Luca, K. Dokova, A. Dramowski, S. J. Dunachie, T. Duong Bich, T. Eckmanns, D. Eibach, A. Emami, N. Feasey, N. Fisher-Pearson, K. Forrest, C. Garcia, D. Garrett, P. Gastmeier, A. Z. Giref, R. C. Greer, V. Gupta, S. Haller, A. Haselbeck, S. I. Hay, M. Holm, S. Hopkins, Y. Hsia, K. C. Iregbu, J. Jacobs, D. Jarovsky, F. Javanmardi, A. W. J. Jenney, M. Khorana, N. Kissoon, E. Kobeissi, T. Kostyanev, K. Phommasone, S. Khusuwan, F. Krapp, R. Krumkamp, A. Kumar, H. H. Kyu, C. Lim, K. Lim, D. Limmathurotsakul, M. J. Loftus, M. Lunn, J. Ma, A. Manoharan, F. Marks, J. May, M. Mayxay, N. Mturi, T. Munera-Huertas, P. Musicha, L. A. Musila, M. M. Mussi-Pinhata, R. N. Naidu, T. Nakamura, R. Nanavati, S. Nangia, P. Newton, C. Ngoun, A. Novotney, D. Nwakanma, C. W. Obiero, T. J. Ochoa, A. Olivas-Martinez, P. Olliaro, E. Ooko, E. Ortiz-Brizuela, P. Ounchanum, G. D. Pak, J. L. Paredes, A. Y. Peleg, C. Perrone, T. Phe, N. Plakkal, A. Ponce-de-Leon, M. Raad, T. Ramdin, S. Rattanavong, A. Riddell, T. Roberts, J. V. Robotham, A. Roca, V. D. Rosenthal, K. E. Rudd, N. Russell, H. S. Sader, W. Saengchan, J. Schnall, J. A. G. Scott, S. Seekaew, M. Sharland, M. Shivamallappa, J. Sifuentes-Osornio, A. J. Simpson, N. Steenkeste, A. J. Stewardson, T. Stoeva, N. Tasak, A. Thaiprakong, G. Thwaites, C. Tigoi, C. Turner, P. Turner, H. R. van Doorn, S. Velaphi, A. Vongpradith, M. Vongsouvath, H. Vu, T. Walsh, J. L. Walson, S. Waner, T. Wangrangsimakul, P. Wannapinij, T. Wozniak, T. E. M. W. Young-Sharma, K. C. Yu, P. Zheng, B. Sartorius, A. D. Lopez, A. Stergachis, C. Moore, C. Dolecek and M. Naghavi, *Lancet*, 2022, **399**, 629–655.

6 S. Kang, H. Qin, L. Zhang, Y. Huang, X. Bai, X. Li, D. Sun, Y. Wang and L. Cui, *Sci. Rep.*, 2017, **7**, 44338.

7 A. Bigham, A. Zarepour, M. Safarkhani, Y. Huh, A. Khosravi, N. Rabiee, S. Iravani and A. Zarrabi, *Nano Mater. Sci.*, 2024, **7**, 1–23.

8 B. C. Ma, S. Ghasimi, K. Landfester and K. A. I. Zhang, *J. Mater. Chem. B*, 2016, **4**, 5112–5118.

9 K. Oka, B. Winther-Jensen and H. Nishide, *Adv. Energy Mater.*, 2021, **11**, 2003724.

10 K. Oka, H. Nishide and B. Winther-Jensen, *Adv. Sci.*, 2021, **8**, 2003077.

11 J. Chen, W. Zhang, L. Wang and G. Yu, *Adv. Mater.*, 2023, **35**, e2210772.

12 H. Shiroma, A. Chikamoto, M. Kameoka, K. Kumagai, H. Matsuyama and Y. Ichihashi, *Res. Chem. Intermed.*, 2025, **51**, 2591–2604.

13 G. Han and Y. Sun, *Mater. Today Phys.*, 2021, **16**, 100297.

14 K. Oka, O. Tsujimura, T. Suga, H. Nishide and B. Winther-Jensen, *Energy Environ. Sci.*, 2018, **11**, 1335–1342.

15 D. Larcher and J. M. Tarascon, *Nat. Chem.*, 2015, **7**, 19–29.

16 K. Okubo, H. Yoshino, H. Miyasaka, H. Kasai and K. Oka, *ACS Appl. Mater. Interfaces*, 2025, **17**, 14561–14568.

17 K. Okubo, S. Kitajima, H. Kasai and K. Oka, *Small*, 2025, **21**, e2410794.

18 C. Strietzel, K. Oka, M. Stromme, R. Emanuelsson and M. Sjodin, *ACS Appl. Mater. Interfaces*, 2021, **13**, 5349–5356.

19 C. N. Gannett, L. Melecio-Zambrano, M. J. Theibault, B. M. Peterson, B. P. Fors and H. D. Abruña, *Mater. Rep.: Energy*, 2021, **1**, 100–149.

20 K. Oka, K. Kamimori, B. Winther-Jensen and H. Nishide, *Adv. Energy Sustainability Res.*, 2021, **2**, 2100103.

21 R. N. Abalos, I. A. Aziz, M. Caverzan, A. S. Lochedino, L. E. Ibarra, A. Gallastegui, C. A. Chesta, M. L. Gomez, D. Mecerreyes, R. E. Palacios and M. Criado-Gonzalez, *Mater. Horiz.*, 2025, **12**, 2524–2534.

22 A. R. L. Caires, T. H. N. Lima and T. F. Abelha, *Mater. Adv.*, 2023, **4**, 1664–1670.

23 Z. Li, W. Lu, S. Jia and H. Yuan, *ACS Appl. Polym. Mater.*, 2021, **4**, 29–35.

24 Q. Jiang, X. Yan, D. Jiao, J. Zhang, Y. Wu and Y. Cheng, *Chem. Commun.*, 2021, **57**, 11244–11247.

25 B. Wang, M. Wang, A. Mikhailovsky, S. Wang and G. C. Bazan, *Angew. Chem., Int. Ed.*, 2017, **56**, 5031–5034.

26 H. Wang, L. Guo, Y. Wang and L. Feng, *Biomater. Sci.*, 2019, **7**, 3788–3794.

27 H. Zhang, Y. Liang, H. Zhao, R. Qi, Z. Chen, H. Yuan, H. Liang and L. Wang, *Macromol. Biosci.*, 2020, **20**, e1900301.

28 A. Lanzilotto, M. Kyropoulou, E. C. Constable, C. E. Housecroft, W. P. Meier and C. G. Palivan, *JBIC, J. Biol. Inorg. Chem.*, 2018, **23**, 109–122.

29 R. D. McCullough, *Adv. Mater.*, 1998, **10**, 93–116.

30 H. Kasai, S. N. Hari, O. Hidetoshi, O. Shuji, M. Hiro, M. Nobutsugu, K. Atsushi, O. Katsumichi, M. Akio and M. Hachiro, *Jpn. J. Appl. Phys.*, 1992, **31**, L1132–L1134.

31 I. Y. Perevyazko, A. Vollrath, C. Pietsch, S. Schubert, G. M. Pavlov and U. S. Schubert, *J. Polym. Sci., Part A: Polym. Chem.*, 2012, **50**, 2906–2913.

32 K. Tanaka, H. Kuramochi, K. Maeda, Y. Takahashi, M. Osako and G. Suzuki, *ACS Omega*, 2023, **8**, 14470–14477.

33 M. Suzuki, H. Kasai, T. Ishizaka, H. Miura, S. Okada, H. Oikawa, T. Nihira, H. Fukuro and H. Nakanishi, *J. Nanosci. Nanotechnol.*, 2007, **7**, 2748–2752.

34 W. Huang and C. Zhang, *Biotechnol. J.*, 2018, **13**, 1700203.

35 H. J. Chen, C. Yang, T. Hang, G. Liu, J. Wu, D. A. Lin, A. Zhang, Y. Li, B. R. Yang and X. Xie, *Sci. Rep.*, 2018, **8**, 12600.

36 J. Hildebrandt and A. F. Thunemann, *Macromol. Rapid Commun.*, 2023, **44**, e2200874.

37 D. M. Scott, A. Nikoubashman, R. A. Register, R. D. Priestley and R. K. Prud'homme, *Langmuir*, 2023, **39**, 570–578.
38 X. Yan, M. Delgado, J. Aubry, O. Gribelin, A. Stocco, F. Boisson-Da Cruz, J. Bernard and F. Ganachaud, *J. Phys. Chem. Lett.*, 2018, **9**, 96–103.
39 J. Müllerová, M. Kaiser, V. Nádaždy, P. Šiffalovič and E. Majková, *Sol. Energy*, 2016, **134**, 294–301.
40 E. Gutiérrez-Fernández, T. A. Ezquerra, E. Rebollar, J. Cui, S. Marina, J. Martín and A. Nogales, *Polymer*, 2021, **218**, 123515.
41 H. D. Kim, Y. Horiuchi, S. Iwasaki, T. Fukuhara and H. Ohkita, *ACS Appl. Mater. Interfaces*, 2021, **13**, 39322–39330.
42 H. M. Feier, O. G. Reid, N. A. Pace, J. Park, J. J. Bergkamp, A. Sellinger, D. Gust and G. Rumbles, *Adv. Energy Mater.*, 2016, **6**, 1502176.
43 S. L. Chua, Y. Ding, Y. Liu, Z. Cai, J. Zhou, S. Swarup, D. I. Drautz-Moses, S. C. Schuster, S. Kjelleberg, M. Givskov and L. Yang, *Open Biol.*, 2016, **6**, 160162.
44 D. A. Bass, J. W. Parce, L. R. Dechatelet, P. Szejda, M. C. Seeds and M. Thomas, *J. Immunol.*, 1983, **130**, 1910–1917.
45 Q. Tian, Y. Jiang, X. Duan, Q. Li, Y. Gao and X. Xu, *Water Res.*, 2025, **268**, 122621.
46 J. Xu, C. Yu, S. Wang, L. Xiong, F. Geng, J. Lv, L. Zhao and Y. Wang, *J. Environ. Chem. Eng.*, 2023, **11**, 110915.
47 L. Hochvaldova, D. Panacek, L. Valkova, R. Vecerova, M. Kolar, R. Prucek, L. Kvitek and A. Panacek, *Commun. Biol.*, 2024, **7**, 1552.
48 M. Tang, H. Yu, J. Deng, F. Ke, Q. Liu, M. Xu, X. Tian, J. Wang, C. Song and X. Guo, *ChemistrySelect*, 2026, **11**, e01427.
49 R. van Grieken, J. Marugán, C. Pablos, L. Furones and A. López, *Appl. Catal., B*, 2010, **100**, 212–220.